CHALMERS
UNIVERSITY OF TECHNOLOGY

Large-eddy simulation study of effects of clearing in forest on wind turbines

6th Symposium on OpenFOAM in Wind Energy
June 13th–14th, 2018, Visby, Sweden

UPPSALA UNIVERSITET

Large-eddy simulation study of effects of clearing in forest on wind turbines

J. Matsfelt[1] and **L. Davidson**[1]

[1]Chalmers University of Technology, Dep. of Mechanics and Maritime Sciences, Div. of Fluid Dynamics, *johanna.matsfelt@chalmers.se*

Abstract. The setup of Ryningsnäs in Sweden is simulated with wind blowing from the south. The inlet boundary planes are used from a precursor that has a length of 5000m to avoid streaks. For the second wind turbine the current clearing has the highest electrical power. In the extended clearing the estimated power is higher than in the homogeneous forest but FAST estimates the opposite. The second turbine in the extended clearing has the lowest rotor torque and RMS values and fatigue loads of the rotor bending around the y-axis and z-axis.

When clearings are present in a forest the flow field is changed dramatically compared to a fully homogeneous forest. But what effects do clearings have on wind turbines located close to them? To find the answer to this question the setup at Ryningsnäs in Sweden is simulated with wind blowing from the south. This because the wind turbine after the clearing will then be within 22 forest heights after the clearing, which is the forest affecting distance [1]. The computational domain seen from above can be seen to the left in Fig. 1. Here the forest is in white and the clearing in grey, also seen is the locations of the two wind turbines at the site. In all the simulations the 5MW wind turbines from NREL is used. An extended clearing is also simulated which has the maximum width of the current clearing along it and reaches the second turbine. This clearing can be seen to the right in Fig. 1. Both the clearings are streamwise larger than five forest heights, which has been shown that leads to that the flow always show edge effects [2]. To be able to distinguish the effects of the clearings a setup with homogeneous forest is also investigated and its domain can be seen in the middle of Fig. 1. All the computational domains has a width of 1000m, a length of 1600m and a height of 800m. The forest is modelled using the model by Shaw and Shumann [3]. The forest at Ryningsnäs site is scots pine tree and has been used to model the vertical area density [4]. The wall model was set to model grass plains below the forest. The simulations was set to simulate neutral stratification. To validate and investigate the implementations in SOWFA the results from the simulations were compared with a measurement campaign [5].

As inlet boundary condition planes from a precursor simulation is used. The precursor simulation is set to have a velocity along the x-axis of 10m/s at hub height of the wind turbines at 90m. All the precursor simulations are using the same width of 1000m and height of 800m of the computational domains. The length is investigated to avoid streaks. The time averaged velocity along the x-axis at planes at hub heigth for the tested computational domain length of 1600m, 3000m, 5000m and 10000m can be seen to the left in Fig. 2. For the two shortest computational domains streaks are clearly seen. The 3000m setup is the shortest length recommended for SOWFA at neutral to lightly unstable stratifications [6]. For this setup with neutral stratification the shortest length is not enough. In the simulations using the two longest computational domains no streaks are seen so both are accepted to be used as inlet boundary condition. The 5000m precursor simulation is chosen as inlet boundary condition because of its less computational

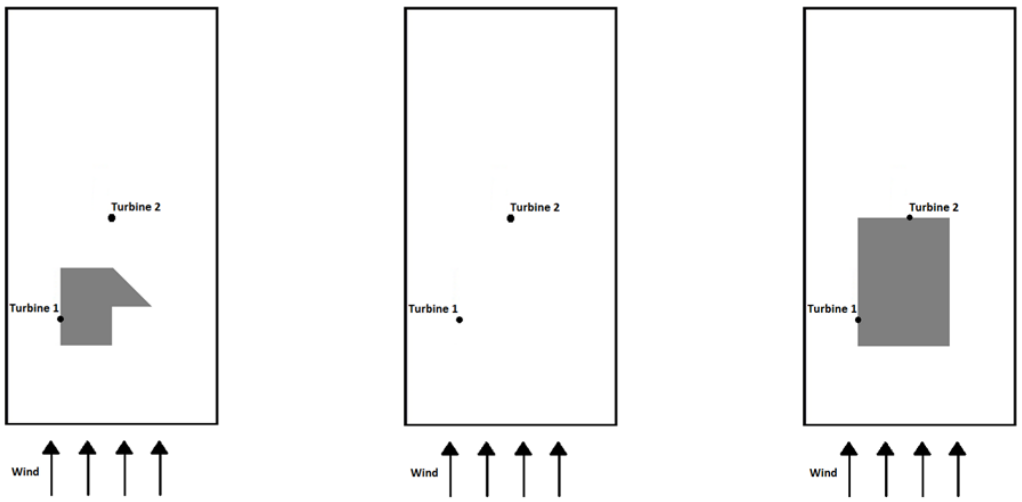

Figure 1: Current (left), Homogen (middle) and Extended (right) computational domains, white is forest and clearing in grey, also seen is the location of the two turbines.

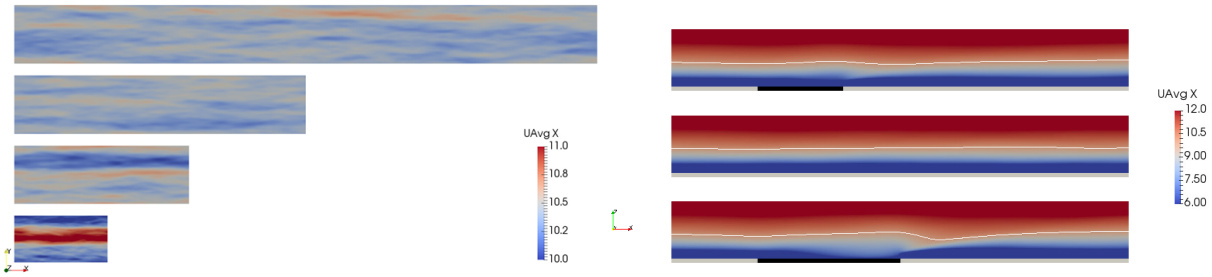

Figure 2: To the left planes of the time averaged velocity along the x-axis for the precursor simulations at hub height. To the right time averaged velocity along x-axis from the atmospheric boundary layer simulations at plane y = 400m. Contour line in white of time averaged velocity along x-axis of 10m/s. From the top current clearing, homogeneous forest and extended clearing. Below each plane the location of the clearing is marked in black.

cost. Despite the need to be careful when chosing the length of the precursor in order to avoid streaks. This kind of dynamic inflow boundary condition outperformed a static inlet boundary condition in LES simulations of an edge flow [7].

To investigate the flow field y-planes at y = 400m of the velocity along the x-axis is seen in Fig. 2, y-axis and z-axis in Fig. 3. The homogeneous forest is located in the middle of each figure and here the wind is blowing along the forest with a constant boundary layer height. The velocity along the x-axis is increasing close to the ground in the downstream part of the extended clearing. In the current clearing the flow is not affected as much by the clearing as in the extended clearing. Downstream the clearings the flow above the forest is accelerating and starting to build a new boundary layer above the forest which is shown by that the white contour line is moving closer to the ground. The velocity along the y-axis is mainly affected in the case of the current clearing when looking at y-planes of y = 400m. This because in this case it is cutting just at the edge of the clearing. At the end of the current clearing the flow is also moving more to the west than what is seen in the case of the extended clearing.

The locations of the turbines are studied in more detail by looking at the normalized horizontal velocity in Fig. 4. Some difference to the measurements are expected since the simulations only take into account

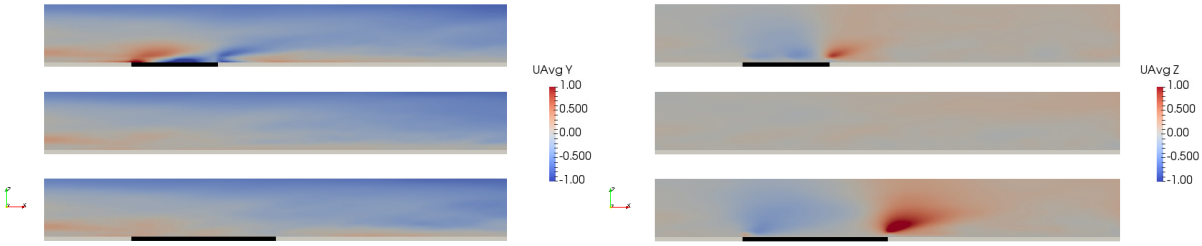

Figure 3: Time averaged velocity along the y-axis to the left and z-axis to the right from the atmospheric boundary layer simulations on a plane at y = 400m. From the top current clearing, homogeneous forest and extended clearing. Below each plane the location of the clearing is marked in black.

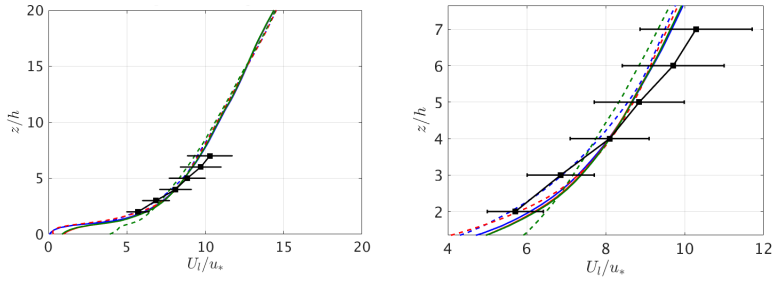

Figure 4: To the left $\langle U_l/u_* \rangle$ from atmospheric boundary layer simulations at the location of the wind turbines and to the right a zoom at the rotor plane. —— : Wind turbine 1 in homogeneous forest, – – : Wind turbine 2 in homogeneous forest, —— : Wind turbine 1 in current clearing, – – : Wind turbine 2 in current clearing, —— : Wind turbine 1 in extended clearing, – – : Wind turbine 2 in extended clearing, —■—: Measurements

wind blowing from the south. The velocity at the first wind turbine is more or less the same in all the simulations. The reason is that the flow has mainly travelled along homogeneous forest before reaching this wind turbine. The velocity profiles for the wind turbine located after the clearing in the homogeneous forest and the current clearing are similar at the bottom and top of the rotor plane. But the homogeneous forest has a more flat velocity profile along the rotor plane. The wind turbine after the clearing in the extended clearing has the highest velocity at the bottom of the rotor plane and the lowest velocity at the top of the rotor plane and thereby the flattest velocity profile of them all. When looking at the velocity along the z-axis to the right in Fig. 3 the flow is moving downwards into the clearing after the forest edge and up after the clearing. This velocity is strongest in the case of the extended clearing because of the clearest disrupting of the forest boundary layer upstream the clearing is seen here. This is consistent with what is observed for the velocity along the x-axis.

The electrical generator power from FAST for the different wind turbines are seen in Table 1. For the atmospheric boundary layer simulation the power is estimated from the one dimensional momentum theory i.e. $\langle U \rangle^3$. For the first wind turbine FAST estimates an higher power than $\langle U \rangle^3$ compared to the second wind turbine in homogeneous forest. No measurements are available, but due to the higher complexity of FAST these results are assumed to be more correct than the estimates using $\langle U \rangle^3$. The estimated power for the second wind turbine is the highest for the atmospheric simulations followed by the simulations with only the second turbine and the simulations with both the wind turbines always give the lowest power. This decrease in power for the second turbine in the simulations with both wind turbines show that the first turbine has some effect on the second turbine when the wind is blowing from the south. For the first wind turbine all the simulations show the same trend. This is also the case for the second wind turbine of the current clearing. But for the second wind turbine in the extended

Electrical Generator Power	Homogenous forest		Current clearing		Extended clearing	
	Turbine 1 (%)	Turbine 2 (%)	Turbine 1 (%)	Turbine 2 (%)	Turbine 1 (%)	Turbine 2 (%)
$\langle U \rangle^3$	+6.9	0.0	+7.0	+4.3	+7.2	+1.2
FAST, Only Turbine 2		0.0		+3.8		-2.6
FAST, Both Turbines	+8.6	0.0	+8.5	+3.0	+8.5	-3.5

Table 1: Estimation of power from the one dimensional momentum theory i.e. $\langle U^3 \rangle$ for the atmospheric boundary layer simulations. Time averaged electrical generator power from simulations with wind turbines.

Rotor torque	Homogenous forest		Current clearing		Extended clearing	
	Turbine 1 (%)	Turbine 2 (%)	Turbine 1 (%)	Turbine 2 (%)	Turbine 1 (%)	Turbine 2 (%)
FAST, Only Turbine 2		0.0		+2.6		-1.8
FAST, Both Turbines	+5.6	0.0	+5.5	+2.0	+5.5	-2.4

Table 2: Time averaged rotor torque i.e. rotor bending moment around the x-axis.

clearing both the FAST simulations show that the power is lower than the second wind turbine in the homogeneous forest. However the atmospheric boundary layer simulation show the opposite. This shows the complexity of the problem and the importance of the FAST coupling.

The bending moment of the rotor has also been investigated using FAST. The time averaged rotor bending around the x-axis i.e. rotor torque can be seen in Table 2. Because of the close relation between power and torque the trends are the same as for the electrical generator power seen in Table 1. For the rotor bending around the y-axis the RMS (root mean square) values are evaluated and presented in Table 3. The difference for the first turbine in the homogeneous forest compared to the current and extended clearings is because the turbine is located in the edge of the forest in the clearing cases. This flattens the velocity profile in the region above the forest which decreases the rotor bending moment around the y-axis. Comparing the second wind turbine for the three different cases show that the current clearing has a bit lower rotor bending moment around the y-axis than the wind turbine in the homogeneous forest. Looking at the horizontal velocity in Fig. 4 it can be seen that the current clearing has a somewhat flatter velocity profile except in the lowest part of the rotor location compared to the homogeneous forest. The extended clearing has the lowest bending moment around the y-axis of them all. It can also be seen that the second wind turbine has the flattest velocity profile i.e. the lowest wind shear seen in Fig. 4. The RMS of the rotor bending around the z-axis can be seen in Table. 4. The trends are the same as for the rotor bending moment around the y-axis.

Rotor bending moment around y-axis	Homogenous forest		Current clearing		Extended clearing	
	Turbine 1 (%)	Turbine 2 (%)	Turbine 1 (%)	Turbine 2 (%)	Turbine 1 (%)	Turbine 2 (%)
FAST, Only Turbine 2		0.0		-0.5		-5.0
FAST, Both Turbines	+2.4	0.0	+1.0	-0.9	+1.0	-5.0

Table 3: RMS of rotor bending moment around the y-axis.

Rotor bending moment around z-axis	Homogenous forest		Current clearing		Extended clearing	
	Turbine 1 (%)	Turbine 2 (%)	Turbine 1 (%)	Turbine 2 (%)	Turbine 1 (%)	Turbine 2 (%)
FAST, Only Turbine 2		0.0		-1.0		-5.2
FAST, Both Turbines	+2.8	0.0	+1.4	-0.8	+1.1	-5.0

Table 4: RMS of rotor bending moment around the z-axis.

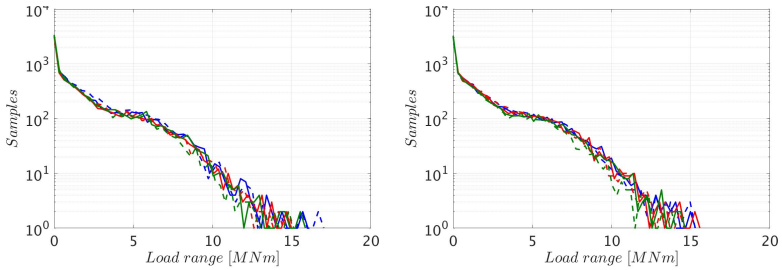

Figure 5: Rain flow of rotor bending moment around the y-axis to the left and z-axis to the right. —— : Wind turbine 1 in homogeneous forest, – – : Wind turbine 2 in homogeneous forest, —— : Wind turbine 1 in current clearing, – – : Wind turbine 2 in current clearing, —— : Wind turbine 1 in extended clearing, – – : Wind turbine 2 in extended clearing

To evaluate the fatigue loads the rain flow counting algorithm is used [8]. The fatigue loads of the rotor torque is not shown since the load range is much lower than what it is for the rotor bending around the y-axis and z-axis seen in Fig. 5. In both these cases the second wind turbine in the extended clearing is generally the one with the lowest loading range.

References

[1] S. Dupont, J.-M. Bonnefond, M. R. Irvine, E. Lamaud, and Y. Brunet, 2011, "Long-distance edge effects in a pine forest with a deep and sparse trunk space: In situ and numerical experiments", Agricultural and Forest Meteorology, vol. 151, pp. 328344.

[2] S. Dupont and Y. Brunet, 2008, "Edge flow and canopy structure: A large-eddy simulation study", Boundary-Layer Meteorology, vol. 126, pp. 5171.

[3] R. Shaw and U. Shumann, 1992, "Large-eddy simulation of turbulent flow above and within a forest", Boundary-Layer Meteorology, vol. 61, pp. 4764.

[4] B. Lalic and D. Mihailovic, 2004, "An empirical relation describing leaf area density inside the forest for environmental modeling", Journal of Applied Meteorology, vol. 43, pp. 641645.

[5] H. Bergström et al., 2013, "Wind power in forests: wind and effects on loads", Vindforsk Rapport, pp. 1167.

[6] M. Churchfield and S. Lee and P. Moriarty, 2012, "Overview of the Simulator of Offshore Wind Farm Application", Webinar, pp. 1-109.

[7] E. Mueller and W. Mell, and A. Simeoni, 2014, "Large eddy simulation of forest canopy flow for wildland fire modeling", Canadian Journal of Forest Reasearch, vol. 44, pp. 15341544

[8] American Society for Testing and Materials, 1985, "Standard practices for cycle counting in fatigue analysis", Technical report.